Polymer 51 (2010) 3801–3807

Contents lists available at ScienceDirect

Polymer

journal homepage: www.elsevier.com/locate/polymer

# Starch-derived carbon aerogels with high-performance for sorption of cationic dyes

Xinhong Chang, Dairong Chen*, Xiuling Jiao

*Key Laboratory of Special Functional Aggregated Materials, Ministry of Education, School of Chemistry and Chemical Engineering, Shandong University, Jinan 250100, PR China*

ARTICLE INFO

*Article history:*
Received 23 November 2009
Received in revised form
27 February 2010
Accepted 5 June 2010
Available online 12 June 2010

*Keywords:*
Starch
Aerogels
Adsorption

ABSTRACT

Environmentally green carbon aerogels have been prepared as adsorbents for dye-containing wastewater. The aerogels were prepared by carbonization of starch aerogels synthesized from soluble starch through a sol–gel process followed by drying at ambient pressure. The Brunauer-Emmett-Teller (BET) surface areas and pore size distribution were measured by $N_2$ adsorption/desorption, and the surface zeta-potential and microstructure of carbon aerogels were characterized using a scanning electron microscope (SEM) and zeta-potential analyzer. SEM images indicate that the carbon aerogels consist of flakes with side length of 60–120 μm and thickness of 3–4 μm. The flakes are irregular in shape and composed of spherical carbon nanoparticles of 10–30 nm. The carbon aerogels have both microporous and mesoporous structures and exhibit high specific surface areas, the highest value is 1571 $m^2/g$. The mean diameter of the micropores is 0.89 nm and that of the mesopores is 2–10 nm. At pH = 10, the carbon aerogels have a zeta-potential of −40 mV and exhibit high adsorption capacities for cationic dyes, such as crystal violet (CV), methyl violet (MV) and methylene blue (MB), from aqueous solution. The largest adsorption capacities for CV, MV and MB are 1515, 1423 and 1181 mg/g, respectively.



## 1. Introduction

As a novel porous material, carbon aerogel, prepared by carbonization of organic aerogels, has attracted considerable attention because of its applications in water purification, gas adsorption, separation of heavy metals and ions, electronic capacitors, fuel cell electrodes, parts for inertial confinement fusion targets, catalyst supports and so on [1–6]. The most widely used organics for the fabrications of aerogels are resorcinol–formaldehyde [7–9], but may also include phenolicfurfural [10,11], polyurethane [12–14], 5-methylresorcinol-formaldehyde [15], and others [16–20]. All of these are man-made polymers, but natural ones including cellulose, alginate, chitosan and starch etc. exhibit some advantages as raw materials to natural materials and carbon aerogels because of their non-toxicity, low cost, and availability [21–27]. To remove solvents from wet-gels, the usual drying method is supercritical $CO_2$ extraction, which is difficult to realize in commercial applications due to the lengthy and dangerous process and high processing cost [28–30]. To decrease the processing cost and shorten the synthesis time, more economical methods such as freeze-, microwave-, and ambient pressure-drying have been developed [9,31–34], and many organic aerogels have been prepared. However, to the best of our knowledge, use of a natural polymer as raw material combined with these economical drying methods has not been reported. Herein, we describe an easy and low-cost route to carbon aerogels by the carbonization of starch aerogels from the corresponding wet-gels through the ambient pressure drying process. The textural characteristics of carbon aerogels can be tailored by adjusting the carbonization temperature and activation time.

Color removal from dye-contaminated wastewaters in the textile, dyeing, printing and other related industries have long been a major environmental problem [35–37]. In the past decades, various methods including adsorption on various sorbents, chemical decomposition by oxidation, photo-degradation, and microbiological decoloration have been used [38–41]. Among these, physical adsorption of dye molecules by porous materials is intensively studied because of the fast kinetics [42]. Thus the adsorption of dye molecules by many natural and synthetic porous materials has been studied and discovery of new, high-performance adsorbents has been pursued. Nevertheless, up to date no significant porous materials have been found to have potential commercial application because of their low adsorption capacities. For example, the largest capacities of the sorbents to crystal violet (CV), methyl violet (MV) and methylene blue (MB) molecules are respectively 500.0, 62.8 and 1000.0 mg/g [43–45], and the sorbents

* Corresponding author. Tel.: +86 0531 88364280; fax: +86 0531 88364281.
*E-mail address:* cdr@sdu.edu.cn (D. Chen).

0032-3861/$ – see front matter © 2010 Elsevier Ltd. All rights reserved.
doi:10.1016/j.polymer.2010.06.018

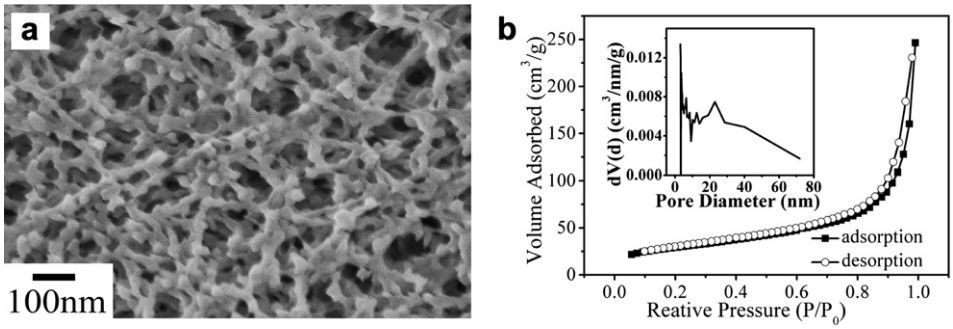


**Fig. 1.** SEM image (a) and $N_2$ adsorption/desorption isotherm (b) of starch aerogel.

used to date cannot be regenerated and reused. In the present work, our experiments showed that starch-derived carbon aerogels exhibited high adsorption capacities for CV, MV and MB dyes from solution and the aerogels can be recycled several times with minimal drop in efficiency.

## 2. Experimental section

### 2.1. Synthesis

In a typical synthesis, 10.0 g of soluble starch was dissolved in 50.0 mL boiling water under stirring to form a translucent solution, which gradually transformed into white wet-gels within 0.5 h. After the wet-gels were aged for 24 h at 25 °C, the solvents were exchanged with absolute acetone. Starch aerogels were prepared by drying the acetone-gels at 50 °C under ambient pressure, then carbonized under $N_2$ flow (100.0 $cm^3$/min) at 850 °C to give carbon aerogels. To adjust their microstructures, the carbon aerogels were activated at 800 °C for different lengths of time under $CO_2$ atmosphere (100.0 $cm^3$/min).

### 2.2. Characterization

The Brunauer-Emmett-Teller (BET) surface area ($S_{BET}$) and pore size distribution (PSD) were measured by $N_2$ adsorption/desorption at 77 K using a QuadraSorb SI surface area analyzer after degassing the samples at 300 °C for 4.0 h. The microstructures of the carbon aerogels were characterized by scanning electron microscopy (SEM, Hitachi S-520, JXA-840), and the zeta (ζ)-potentials were measured with a ζ-potential analyzer (Zeta-plus, Shanghai Instruments Corp.). A pH meter (PHS-2) was applied to determine the pH of the solutions. The Fourier transform infrared (FT-IR) spectra were recorded on a FT-IR spectrometer (Nicolet 5DX) using the KBr pellet method in the range 400–4000 $cm^{-1}$. Thermogravimetric (TG) analysis was conducted in a $N_2$ atmosphere at a heating rate of 10.0 °C/min from 50 °C to 1000 °C (TA's SDTQ600 thermal-analyzer).

### 2.3. Boehm's titrations

The amounts of different surface acidic functional groups in carbon aerogels were determined by Boehm's method. For

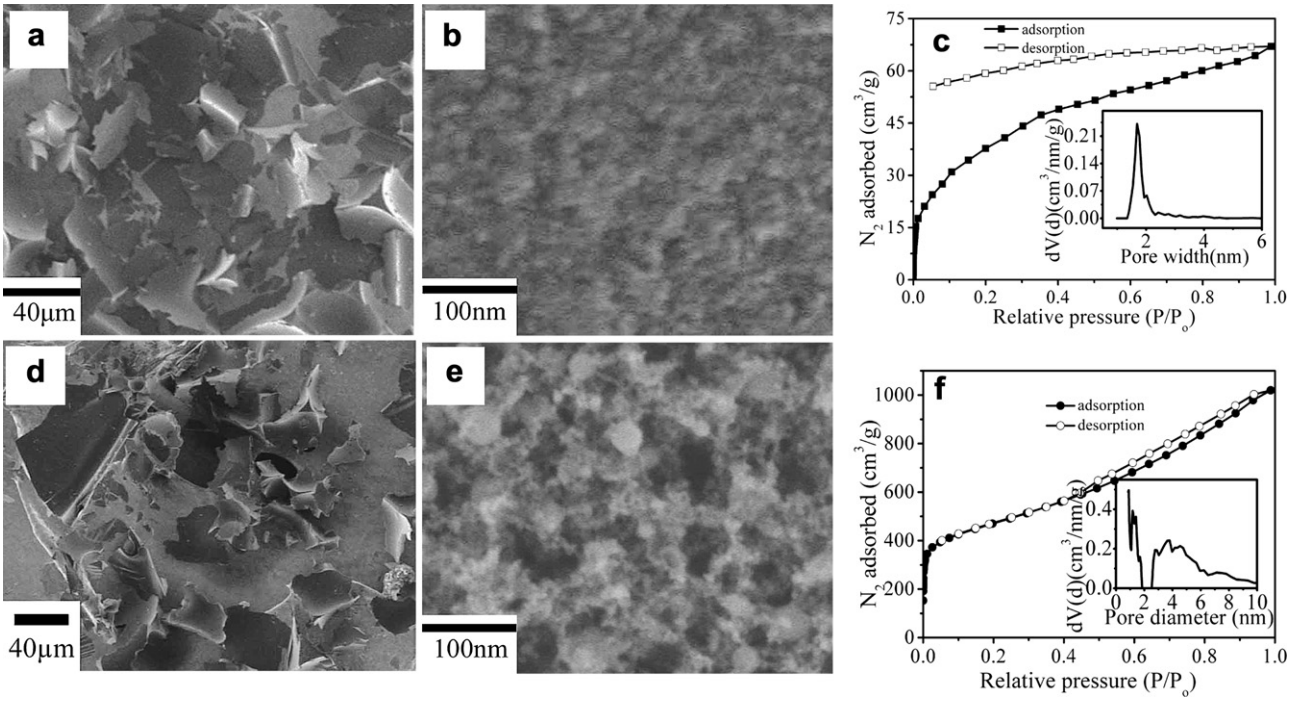


**Fig. 2.** SEM images at (a) low magnification and (b) high magnification and $N_2$ adsorption/desorption isotherm (c) of carbon aerogel before activation (Sample 1 in Table 1). SEM images (d) low magnification and (e) high magnification and $N_2$ adsorption/desorption isotherm (f) of carbon aerogel activated at 800 °C for 7.0 h (Sample 5 in Table 1).

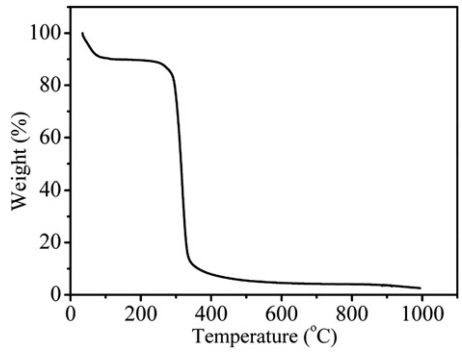


**Fig. 3.** TG curve of starch aerogel.

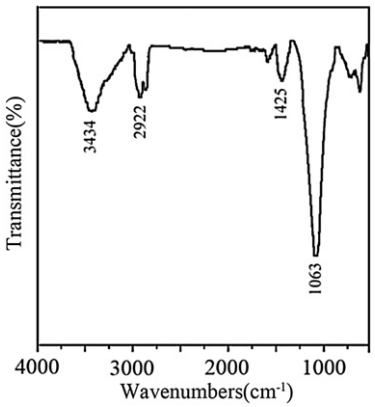


**Fig. 4.** IR spectrum of activated carbon aerogel (sample 5 in Table 1).

a sample, 0.5 g of dry carbon aerogel was weighed into 100.0 mL conical flask prior to the addition of 50.0 mL of base with varying strength, e.g., 0.1 mol/L solution of sodium hydrogen carbonate, sodium carbonate and sodium hydroxide. Carbon aerogel samples were agitated for 72 h at room temperature. The solutions were separated using 0.45 μm PTFE syringe top filters. 10.0 mL aliquots were then titrated with 0.1 mol/L hydrochloric acid using methyl-red as the indicator. High-purity water was used in all titration experiments.

### 2.4. Adsorption measurements

#### 2.4.1. Effect of pH on adsorption

The adsorption of dye molecules was investigated over the pH range of 2–10, which was adjusted with 0.1 M HCl or NaOH. The carbon aerogels (10.0 mg) were added into the dye solution (50.0 mL, 500 ppm) and the mixture was shaken at 25 °C for 24 h until the adsorption reached equilibrium. After filtration through a 0.45 μm membrane filter to remove aerogel particles, the dye concentration in the filtrate was determined by UV–vis absorption (UV-3100, Shimadzu) at 590, 582 and 665 nm for CV, MV and MB, respectively. The amount of adsorbed dye was calculated based on the following equation: $q_e = (C_0 - C_e) \times V/m$, in which $q_e$ is the amount of as-absorbed dyes (mg/g) at equilibrium, $C_0$ and $C_e$ are the initial and residual concentrations at equilibrium (mg/L), $V$ is the volume of dye's solution (L), and $m$ is the dose of carbon aerogel (g).

#### 2.4.2. Adsorption kinetics

Adsorption kinetics experiments were carried out on 1000.0 mL dye solution (50 ppm) mixed with 0.2 g of carbon aerogels in a stoppered Erlenmeyer flask and shaken on a rotary shaker at 200 rpm. Several milliliters of solution were sampled with a pipette at various time intervals. The sample solution was immediately filtered through a 0.45 μm membrane filter and the UV absorbance of the filtrate was measured to determine the dye concentration as above.

**Table 1**
Textural properties of carbon aerogels.

| Sample | SA ($m^2$/g) | PD (nm) | PV ($cm^3$/g) | MSA ($m^2$/g) | MV ($cm^3$/g) | MSAR (%) | MVR (%) |
|---|---|---|---|---|---|---|---|
| 1 CA | 137 | 1.54 | 0.088 | 64 | 0.031 | 47 | 35 |
| 2 ACA–1h | 892 | 0.899 | 0.553 | 545 | 0.277 | 61 | 50 |
| 3 ACA–3h | 1275 | 0.899 | 0.976 | 527 | 0.265 | 41 | 27 |
| 4 ACA–5h | 1348 | 0.899 | 1.021 | 539 | 0.238 | 40 | 23 |
| 5 ACA–7h | 1571 | 0.899 | 1.22 | 601 | 0.29 | 38 | 24 |
| 6 ACA–9h | 1273 | 0.899 | 1.138 | 453 | 0.228 | 36 | 20 |

SA: surface area, PD: pore diameter, PV: pore volume, MSA: micropore surface area, MV: micropore volume, MSAR: micropore surface area ratio percent, MVR: micropore volume ratio percent.

#### 2.4.3. Adsorption isotherms

Adsorption isotherms were determined by measuring the depletion of the dye concentration after the adsorption reached equilibrium at 25 °C. For these experiments, the carbon aerogels (10.0 mg) were added into dye solutions (50.0 mL) of different concentrations with a pH value of 10 and shaken until the equilibration time determined for each material from the kinetics experiments.

#### 2.4.4. Elution of adsorbed dyes

To remove the adsorbed dyes, the carbon aerogels (10.0 mg) with adsorbed dyes were placed in absolute ethanol (50.0 mL) and shaken for 0.5 h at 25 °C. The amount of eluted dyes was determined by measuring the absorbance of the solution. After elution of the dyes with absolute ethanol, the aerogels were recovered by soaking in water for 24 h and they could then be reused to adsorb the dyes as described above.

## 3. Results and discussion

The SEM image shows that the starch aerogel (Fig. 1a) has a three-dimensional continuous network structure, and its specific surface area calculated based on the BET model is 103.0 $m^2$/g. The $N_2$ adsorption/desorption isotherm indicates that the aerogels have a PSD ranging from 3 to 80 nm (Fig. 1b). The starch molecule is composed of α-D-glucose units linking through the α-1, 4 or α-1, 6-glycosidic bond [46]. In water, the starch granules adsorb water and expand, and the chains of starch molecules stretch to form a network structure. The expansion and shrinkage of the starch granules due to the adsorption and desorption of water molecules is reversible as long as the hydrogen bonds between the molecules are intact. At higher temperatures, the association of water molecules through hydrogen bonds decrease, and the water molecules infiltrate near the starch micro-crystals which destroys the hydrogen bonds between the starch molecules. The removal of the hydrogen bonds leaves the starch molecules free to hydrate and the starch network structures adsorb a large number of water molecules, resulting in a great expansion. In this process, water molecules encroach into the molecular chains of starch to interrupt them as the starch solution is heated to 90–100 °C. The formation of a hydrated layer around the separated starch molecules results in complete separation of the molecular chains and the hydration reaction occurs, forming a semi-transparent sol, which is also called a paste. In this process, the viscosity of the dispersed starch solution rapidly increases and maintains a certain value as the temperature decreases. When the starch concentration increases to a certain level, the solution transforms into a gel in which the water

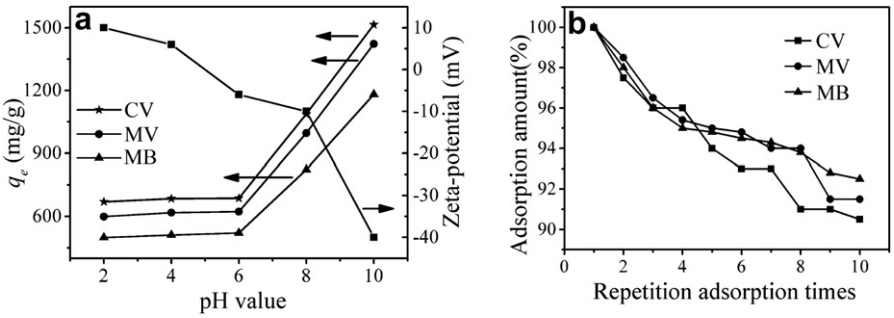


**Fig. 5.** Effects of pH on the adsorption capacities and zeta-potential of carbon aerogels (a), and the adsorption capacities of the carbon aerogels after repeated regeneration cycles at pH = 10 (b).

molecules are fixed. After the starch paste is cooled to room temperature, the starch molecules self-arrange, and the hydrogen bonds between the adjacent molecules gradually lead to the formation of a compact bundle of micro-starch molecules. The aging process does not make the starch completely recover its original structure, rather the molecules form gel networks by winding into double helices. Due to the wide distribution of the molecular weight of starch (32 000–160 000), that is, the difference in the chain length is very large, the PSD in the resulting starch aerogels is correspondingly wide.

After the starch aerogels were carbonized in a $N_2$ atmosphere, carbon aerogels were obtained. SEM images indicate that the carbon aerogels consist of the flakes with side of 60–120 μm and thickness of 3–4 μm (Fig. 2a,d), which have the mesopores composed of carbon nanoparticles of 10–30 nm (Fig. 2b,e). The $N_2$ adsorption measurements indicate that the specific surface area of carbon aerogel is 137 $m^2/g$ and the average pore size is 1.54 nm. According to the Barret-Jovner-Halenda PSD, only few mesopores exist. It should be noted that the hysteresis loop in Fig. 2c is not closed, illustrating that the pores are unstable, which might be due to the compound impurity of decomposed starch existing on the pore walls. The adsorption isotherms show high uptake at very low relative pressure, which is characteristic of microporous materials. The isotherms also exhibit an increasing uptake as the relative pressure increases and a broad hysteresis (the desorption isotherm lies above the adsorption one). Unlike those of mesoporous materials, the hysteresis loop here extends to very low relative pressure, which might be due to its complex micropore structure (arising from a complex distribution of free volume) and/or reorganization and swelling of the carbon upon $N_2$ adsorption [47]. In the activation process, the compound impurity would be oxidized to decompose, which makes the blocked pores re-open and the structure stability of pores increases, thus the hysteresis loop is closed (Fig. 2c).

Fig. 3 shows TG curve of starch aerogel. The process of physical dehydration occurs below 150 °C, and the structure of the chain has no change. The carbonization of a polysaccharide occurs by a liquid process followed by an in situ pyrolysis reaction which is conducted at less than 500 °C. Since the polysaccharide is a complex organic molecule, the starting carbonization temperature is relatively low. At 150 °C the bonded water begins to be lost, and gradually aldehydes and enols are formed. As the temperature increases, a series of changes occur and the molecular chains break with further loss of bonded water, and carbon oxides (CO and $CO_2$) and other small volatile molecules are generated. Around 300 °C, the starch liquefies and aromatization occurs, forming benzene rings. By 500 °C the aromatics dehydrogenate and condense to form the carbonaceous materials through carbonization. Pyrolysis generates low-molecular-weight compounds which are lost to the atmosphere, while in the liquid phase the aromatization and polycondensation take place and the viscosity of the materials increases. One intermediate phase in the process is the condensed aromatic ring structure as a liquid crystal which produces the layered carbon order observed in the products [48].

After the carbon aerogels are activated in $CO_2$ atmosphere, their microstructures would change dramatically (Fig. 2b,e) because the carbon surface can be eroded, and the thin walls between the pores also be oxidized to result in the pores expanding, which exhibit higher mesoporosity than that of before activation. Further experiments indicate that the suitable activation conditions could increase the specific surface areas and pore volume of carbon aerogels (Table 1), and simultaneously create some new micro/mesoporous structures. The average size of the micropores in the carbon aerogels after activation is 0.89 nm, and the mesopore size is in the range of 2–10 nm. The largest specific surface area of 1571 $m^2/g$ is obtained for the carbon aerogel activated at 800 °C for 7.0 h (Fig. 2d). At shorter activation times (from 1.0 to 7.0 h), the corresponding pore volume increases from 0.553 to 1.22 $cm^3/g$, and the ratio of micropore surface area to the total decreases from 61% to

**Table 2**
Amount of acidic groups and amount of dye adsorbed of carbon aerogels surface.

| Samples | Amount of acidic groups (mmol/g) | | | Amount of dye adsorbed (mg/g) | | |
|---|---|---|---|---|---|---|
| | Carboxyl | Lactone | Hydroxyl | CV | MV | MB |
| 1 | 0.25 | 0.15 | 0.38 | 286 | 253 | 236 |
| 2 | 0.32 | 0.19 | 0.38 | 586 | 533 | 512 |
| 3 | 0.36 | 0.21 | 0.39 | 853 | 846 | 832 |
| 4 | 0.39 | 0.23 | 0.50 | 1238 | 1186 | 1069 |
| 5 | 0.41 | 0.25 | 0.62 | 1515 | 1423 | 1181 |
| 6 | 0.52 | 0.26 | 0.54 | 1322 | 1289 | 1098 |

Initial concentration and pH of dyes solution are 500 ppm and 10, respectively.

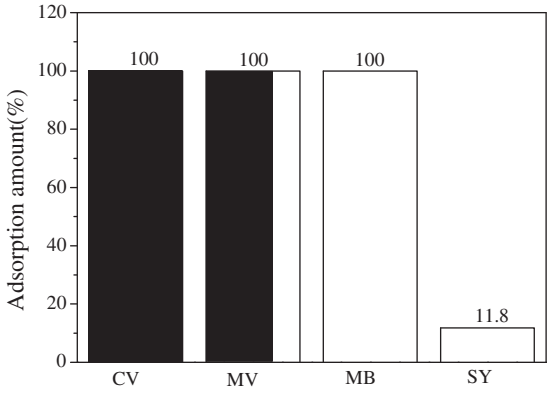


**Fig. 6.** The adsorption capacity of carbon aerogels for CV, MV, MB and SY (50 ppm, pH = 10).

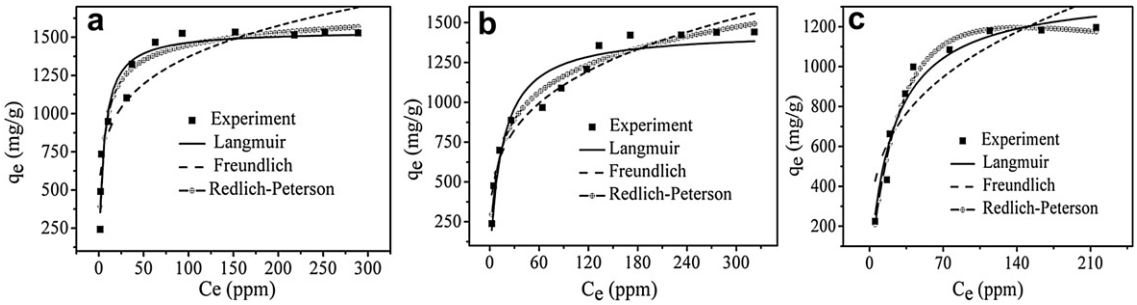


**Fig. 7.** Fits to the experimental adsorption isotherm data by the Langmuir, Freundlich and Redlich–Peterson isotherms CV (a), MV (b) and MB (c).

38%. Moreover, prolonging the activation time to 9.0 h causes the specific surface area to decrease to 1273 $m^2/g$. The ratio of the micropore surface area to the total surface area decreases to 36% because of the disappearance of some mesopores after long-time $CO_2$ oxidation.

The activated carbon aerogels exhibit higher surface negative charges than that activated carbon graininess [49] due to the carboxyl, lactones, hydroxyl and/or carbonyl groups existing on the carbon particle's surface [50]. The ξ-potential of a carbon aerogel dispersion in solution at pH 10 is −40.0 mV, and increased as the pH of the solution decreases, until it reaches the equi-potential point at pH 5.2. Below pH 5.2, the carbon aerogels are positively charged. The IR spectrum of activated carbon aerogel (Fig. 4) shows the absorption bands at 1063, 3434, 2922, and 1425 $cm^{-1}$, indicating that there are $OH^-$ and $COO^-$ groups on the surface of the carbon aerogels under alkaline conditions, so the negative charge would increase with the pH. The pH of the dye solution considerably affects the adsorption of basic dyes on the carbon aerogels (Fig. 5a), and the adsorption capacities change with the pH. At an initial pH of 10 for the dye solution and a dye concentration of 500 ppm, the adsorption capacity is the largest. The maximum adsorption capacities for CV, MV and MB are respectively 1515, 1423 and 1181 mg/g. At pH 6, the adsorption capacities reduce to 670, 599 and 499 mg/g. Considering that the dyes are positively charged and the adsorption capacities in solutions with a pH value of 6–10 increase with the carbon aerogels' negative charge density, the electrostatic sorbent–sorbate interaction might be one of the most important parameters in the dye adsorption. Even though the activated carbon aerogels exhibit a positive charge at pH <5 the dye molecules could still be adsorbed on their surfaces, which might be due to the formation of hydrogen bonds between the surface oxides of the carbon particles and the dye molecules [51]. Previous research has shown that the largest adsorption capacities of activated carbon for CV, MV and MB are respectively 63.53, 0.202 and 580 mg/g [52–54]. The carbon aerogels exhibiting the higher adsorption capacities may due to the high specific surface areas and high negative charges on the surfaces.

In order to further study the adsorption mechanism of dyes on the surface of carbon aerogels, the amount of acidic groups on the surface of carbon aerogels was determined by Boehm titration. Table 2 shows the corresponding results, from sample 1 to 5, the amount of acidic groups increases gradually, and the amount of dyes adsorbed also increases. From sample 5 to 6, the amount of carboxyl groups increases and that of hydroxyl groups decreases. Table 1 shows the surface areas of carbon aerogels increase from sample 1 to 5, and decrease from sample 5 to 6. So we believe both the amount of acidic groups and surface areas of carbon aerogels influence the adsorption of dyes on carbon aerogels. As a comparison, the adsorption capacities of carbon aerogels for the anionic dye sunset yellow (SY) are measured (Fig. 6). The results show that the maximum adsorption capacity is only 11.8%, indicating that the adsorption of activated carbon aerogels for the cationic dye is mainly due to the electrostatic attraction, but also the hydrogen bonds.

Regeneration experiments show that more than 99% of as-adsorbed dyes were removed from the carbon aerogels after being eluted in absolute ethanol for 0.5 h. When the carbon aerogels were reused to adsorb the dye molecules, 90% of the original capacity still remained after 9 cycles (Fig. 5b), showing high stability of the aerogels. The attachment of the dye molecules to the sorbent was weaker than that of the ethanol molecules, so more than 99% of the adsorbed dyes were desorbed. This result demonstrates an efficient regeneration property for the removal and recovery of basic dyes.

The equilibrium adsorption isotherm is of importance in the design of adsorption systems. Several isotherm equations are available and three important isotherms were selected in this study: the Langmuir, Freundlich and Redlich–Peterson isotherms. Fig. 7 shows curve fits to the adsorption isotherms for all three adsorption isotherm models and Table 3 lists the correlation parameters and fitting factors. For adsorption of all three cationic dyes, although the Redlich–Peterson model is the best model for simulation of the adsorption isotherm (as evident from the correlation coefficients $R^2$) [55], it does not well fit the actual adsorption process, which indicates that the actual adsorption process is complex and the simple empirical models cannot be applied to accurately describe the actual adsorption process because that the ionic strength and pH value of the dye solutions might change in the actual adsorption process. Equilibrium constants of Langmuir model or Freundlich model in most cases are dependent of solution chemistry, thus they could not give the fundamental understanding

**Table 3**
The parameters and fitting factors of the isotherm models for the adsorptions of cationic dyes.

| | Langmuir isotherm model | | | Freundlich isotherm model | | | Redlich–Peterson isotherm model | | | |
|---|---|---|---|---|---|---|---|---|---|---|
| | $q_o$ (mg/g) | $K_L$ (L/mg) | $R^2$ | $K_F$ (mg/g) | $n$ | $R^2$ | $K_r$ | $a_r$ | $\beta$ | $R^2$ |
| CV | 1543.53 | 0.1861 | 0.952 | 546.16 | 5.0014 | 0.860 | 358.04 | 0.2983 | 0.9501 | 0.959 |
| MV | 1448.38 | 0.0659 | 0.938 | 332.60 | 3.7394 | 0.950 | 217.25 | 0.3677 | 0.8357 | 0.975 |
| MB | 1383.99 | 0.0436 | 0.959 | 255.85 | 4.8198 | 0.840 | 450.15 | 2.4210 | 0.8886 | 0.978 |

Langmuir, Freundlich and Redlich–Peterson models are expressed as $q_e = q_0(K_L C_\epsilon/(1 + K_L C_\epsilon))$, $q_e = K_F C_\epsilon^{1/n}$ and $q_e = K_r C_\epsilon/(1 + \alpha_r C_\epsilon^{\beta})$, $q_e$(mg/g): dye adsorption capacity, $C_\epsilon$ (ppm): dye concentration at the adsorption equilibrium, $q_0$ (mg/g): a single-layer adsorption capacity, β: index (0–1), $K_L$, $K_F$, $n$, $K_r$ and $\alpha_r$: the constants.

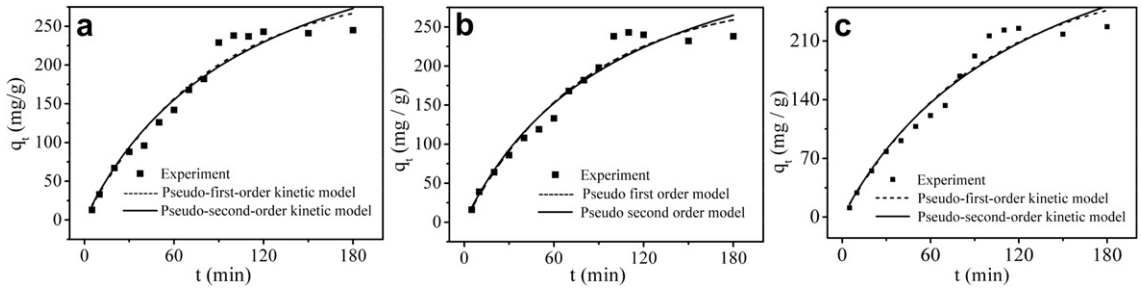


**Fig. 8.** Fits to the experimental data by pseudo-first-order and pseudo-second-order kinetic models. CV (a), MV (b) and MB (c). The pH value of solution is 10.

**Table 4**
The parameters and fitting factors for the adsorptions of dyes on activated aerogels (Temperature: 25 °C, adsorbent concentration: 0.2 g/L, the initial dye concentration: 50 mg/L, pH = 10.0).

| | Pseudo-first-order | | | Pseudo-second-order | | |
|---|---|---|---|---|---|---|
| | $q_e$ (mg/g) | $k_1$ (1/min) | $R^2$ | $q_e$ (mg/g) | $K_2$ (g/mg•min) | $R^2$ |
| CV | 299.10 | 0.0123 | 0.965 | 440.72 | 0.00002 | 0.961 |
| MV | 288.61 | 0.0126 | 0.962 | 421.10 | 0.00002 | 0.959 |
| MB | 287.93 | 0.0107 | 0.962 | 436.25 | 0.00002 | 0.961 |

Pseudo-first-order and pseudo-second-order models are expressed as $q_t = q_e(1 - e^{-k1t})$ and $q_t = k_2 q_e^2 t(1 + k_2 q_e t)$, $k_1$ and $K_2$ are the dynamics constants.

on adsorption process and may not be valid as the solution chemistry is changed [56,57]. The adsorption of dye molecules results in the change of pH value and ionic strength of solution, so that these models are not fitted well.

Two kinetic models (pseudo-first-order equation and pseudo-second-order equation) were applied to investigate the adsorption kinetic processes of the cationic dyes on the carbon aerogels. Fig. 8 illustrates the comparison between the calculated and measured results for adsorption of the dyes on the carbon aerogels, indicating that the adsorption equilibriums were established within 90 min for all three cationic dyes. The parameters and fitting factors ($R^2$) demonstrate the two models do not well fit the actual adsorption dynamics process (Table 4), although the pseudo-first-order model curves are closer to the experimental data than the pseudo-second-order model, indicating that the complex actual adsorption process might include chemical adsorption, physical adsorption and hydrogen bonds adsorption. As the empirical models, these two equations were suitable to the simple adsorption process [58,59], thus there are some differences in the theoretical and experimental results. The adsorption mechanism and kinetics of cationic dyes on carbon aerogels is complex and needs to further be investigated.

## 4. Conclusions

Carbon aerogels derived from starch aerogels have been prepared by use of a relatively simple and green method in which starch wet-gels were prepared within a short time and subsequent ambient pressure drying was applied to generate the starch aerogels. The as-prepared carbon aerogels exhibit a good adsorption performance for CV, MV and MB and it is technically feasible to use this material to remove dye molecules from wastewater. As a good biocompatible polymer, soluble starch is a low cost starting material which has extensive applications in pharmacology, biomedicine, agriculture, and food [60–63]. This research could extend the application of starch in water treatment industries and environmental protection.

## Acknowledgments

This work is supported by a grant from the Major State Basic Research Development Program of China (973 Program) (No. 2010CB933504) and the Doctoral Foundation of Shandong Province (2007BS04042). The authors thank Dr. Pamela Holt for editing the manuscript for English.

## References

[1] Bekyarova E, Kaneko K. Adv Mater 2000;12:1625–8.
[2] Lee J, Lee D, Oh E, Kim J, Kim Y, Jin S, et al. Angew Chem Int Ed Engl 2005;44:7427–32.
[3] Lee J, Kim J, Hyeon T. Adv Mater 2006;18:2073–94.
[4] Du H, Gan L, Li B, Wu P, Qiu Y, Kang F, et al. J Phys Chem C 2007;111:2040–3.
[5] Fairén-Jiménez D, Carrasco-Marín F, Moreno-Castilla C. Langmuir 2007;23:10095–101.
[6] Kwon S, Kim H, Jin H. Polymer 2009;50:2786–92.
[7] Pekala RW. J Mater Sci 1989;24:3221–7.
[8] Al-Muhtaseb SA, Ritter JA. Adv Mater 2003;15:101–14.
[9] Mulik S, Sotiriou-Leventis C, Leventis N. Chem Mater 2007;19:6138–44.
[10] Pekala RW, Alviso CT, Lu X, Gross J, Fricke J. J Non-Cryst Solids 1995;188:34–40.
[11] Wu D, Fu R. Microporous Mesoporous Mater 2006;96:115–20.
[12] Biesmans G, Mertens A, Duffours L, Woignier T, Phalippou J. J Non-Cryst Solids 1998;225:64–8.
[13] Biesmans G, Randall D, Francais E, Perrut M. J Non-Cryst Solids 1998;225:36–40.
[14] Rigacci A, Marechal JC, Repoux M, Moreno M, Achard P. J Non-Cryst Solids 2004;350:372–8.
[15] Pérez-Caballero F, Peikolainen AL, Uibu M, Kuusik R, Volobujeva O, Koel M. Micropor Mesopor Mater 2008;108:230–6.
[16] Li W, Lu A, Guo S. Carbon 2001;39:1989–94.
[17] Li W, Reichenauer G, Fricke J. Carbon 2002;40:2955–9.
[18] Yamashita J, Ojima T, Shioya M, Hatori H, Yamada Y. Carbon 2003;41:285–94.
[19] Zhang R, Li W, Liang X, Wu G, Lü Y, Zhan L, et al. Micropor Mesopor Mater 2003;62:17–27.
[20] Zhang R, Lu Y, Zhan L, Liang X, Wu G, Ling L. Carbon 2003;41:1660–3.
[21] Tan C, Fung BM, Newman JK, Vu C. Adv Mater 2001;13:644–6.
[22] Mukai SR, Tamitsuji C, Nishihara H, Tamon H. Carbon 2005;43:2618–41.
[23] Valentin R, Horga R, Bonelli B, Garrone E, Di R, Quignard F. Biomacromolecules 2006;7:877–82.
[24] Chang X, Chen D, Jiao X. J Phys Chem B 2008;112:7721–5.
[25] Xu C, Luo X, Lin X, Zhuo X, Liang L. Polymer 2009;50:3698–705.
[26] Feng Z, Shao Z, Yao J, Huang Y, Chen X. Polymer 2009;50:1257–63.
[27] Wang Y, Steinhoff B, Brinkmann C, Alig I. Polymer 2008;49:1257–65.
[28] Miao Z, Ding K, Wu T, Liu Z, Han B, An G, et al. Micropor Mesopor Mater 2008;111:104–9.
[29] Qin G, Guo S. Carbon 1999;37:1199–205.
[30] Kruk M, Jaroniec M. Chem Mater 2001;13:3169–83.
[31] Tamon H, Ishizaka H, Yamamoto T, Suzuki T. Carbon 2000;38:1099–105.
[32] Yamamoto T, Nishimura T, Suzuki T, Tamon H. Drying Technol 2001;19:1319–33.
[33] Leonard A, Job N, Blacher S, Pirard JP, Crine M, Jomaa W. Carbon 2005;43:1808–11.
[34] Job N, Panariello F, Marien J, Crine M, Pirard JP, Leonard A. J Non-Cryst Solids 2006;352:24–34.
[35] Tonanon N, Wareenin Y, Siyasukh A, Tanthapanichakoon W, Nishihara H, Mukai SR, et al. J Non-Cryst Solids 2006;352:5683–6.
[36] Karcher S, Kornmuller A, Jekel M. Dyes Pigm 2001;51:111–25.
[37] Koyuncu I. Desalination 2002;143:243–53.
[38] Netpradit S, Thiravetyan P, Towprayoon S. Water Res 2003;37:763–72.
[39] Forgacs E, Cserháti T, Oros G. Environ Int 2004;30:953–71.
[40] Konstantinou IK, Albanis TA. Appl Catal B 2004;49:1–14.

[41] Vanhulle S, Trovaslet M, Enaud E, Lucas M, Taghavi S, van der Lelie D, et al. Environ Sci Technol 2008;42:584–9.
[42] Martínez-Huitle CA, Brillas E. Appl Catal B Environ 2009;87(3/4):105–45.
[43] Wu J, Liu C, Chu K, Suen S. J Memb Sci 2008;309:239–45.
[44] Otero M, Rozada F, Calvo LF, García AI, Morán A. Dyes Pigm 2003;57:55–65.
[45] Doğan M, Özdemir Y, Alkan M. Dyes Pigm 2007;75:701–13.
[46] Özacar M, Şengil İA. J Environ Manage 2006;80:372–9.
[47] Zhang L. Modified materials from natural polymers and their applications [in Chinese]. Beijing: Chemistry Industry Press; 2006. p. 216.
[48] Ghanem BS, McKeown NB, Budd PM, Selbie JD, Fritsch D. Adv Mater 2008;20:2766–71.
[49] O'Connell C. Thermochim Acta 1999;340/341:183–94.
[50] Xiao J, Zhang Y, Wang C, Zhang J, Wang C. Carbon 2005;43:1032–8.
[51] Zhang N, Wang L, Liu H, Cai Q. Surf Interface Anal 2008;40:1190–4.
[52] Chingombe P, Saha B, Wakeman RJ. Carbon 2005;43:3132–43.
[53] Önal Y. J Hazard Mater 2006;137:1719–28.
[54] Iqbal MJ, Ashiq MN. J Hazard Mater 2007;139:57–66.
[55] El Qada EN, Allen SJ, Walker G. Chem Eng J 2006;124:103–10.
[56] Chen J, Yoon J, Yiacoumi S. Carbon 2003;41:1635–44.
[57] Chen J, Lin M. Water Res 2001;35:2385–94.
[58] Chandra TC, Mirna MM, Sudaryanto Y, Ismadji S. Chem Eng J 2007;127:121–9.
[59] Liu Y, Liu Y. Separ Purif Tech 2008;61:229–42.
[60] Chielhi E, Solaro R. Adv Mater 1996;8:305–13.
[61] Zhang L. Starch 2001;53:401–7.
[62] Xu S, Wang J, Wu R, Wang J, Li H. Chem Eng J 2006;117:161–7.
[63] Bravo-Osuna I, Ferrero C, Jiménez-Castellanos MR. Eur J Pharm Biopharm 2008;69:285–93.